Examining the neutral phase circumgalactic medium of NGC 891 NGC 4565

Research Thesis

A thesis submitted in partial fulfillment for graduation with Research Distinction
in Astronomy and Astrophysics in the undergraduate colleges
of The Ohio State University

by

Mary Rickel

Project Advisor: Professor Smita Mathur
Department of Astronomy and Astrophysics

THE OHIO STATE UNIVERSITY

April 2024

THE OHIO STATE UNIVERSITY

Abstract

Smita Mathur
Department of Astronomy and Astrophysics

by Mary Rickel

Work done by Das 2020 (D20 [1]) shows, along the minor axis, the velocity is consistent with an inflow/fountain in NGC 891 and an inflow/outflow in NGC 4565. Previous work done by Das 2024 (D24[2]) along the major axis shows the diffuse H I is a co-rotating CGM or the outer part of an extended HI disk. From D20 and D24, the star formation of NGC 4565 can be sufficiently explained including the circumgalactic H I , the depletion time, and the accretion rate. However, most accreting material in NGC 891 is missing. To obtain a 360° view, we probe the diffuse neutral circumgalactic medium (CGM) along the off axes of NGC 891 and NGC 4565 out to 30 kpc using the Green Bank Telescope (GBT). We detect HI with varying spectral shapes, velocity widths, and column densities with a sensitivity of 10^{16} cm^{-2} . We compare our single-dish detections to the interferometric maps from the Westerbork Synthesis Radio Telescope (WSRT) obtained as part of the HALOGAS survey. We find that all of the emission detected by the GBT cannot be explained by the emission seen in WSRT maps.

Acknowledgements

I would like to express my sincerest gratitude to Dr. Sanskriti Das for her invaluable mentorship over the past two years. Her dedication and passion towards mentoring inspired my sense of belonging in astronomy and motivated me to pursue graduate school. Thank you, Sanskriti, for your unwavering support and belief in me. I am also deeply grateful to Professor Smita Mathur for her guidance, support, and encouragement throughout my academic journey. Special thanks to Professor Adam Leroy for his insightful discussions and role on my thesis defense panel.

Contents

List of Figures

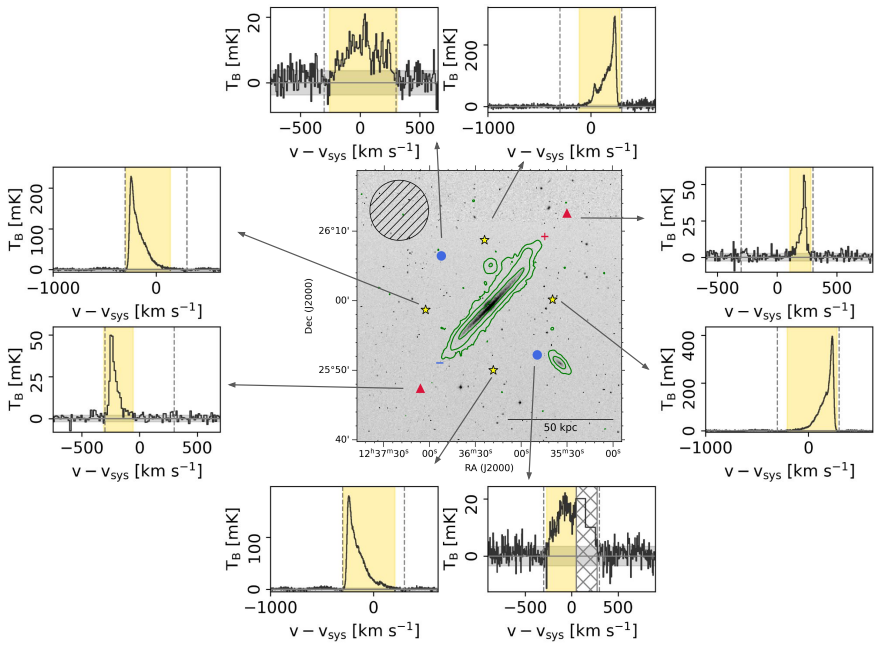

FIGURE 1: NGC 4565 GBT spectra. Red triangle, yellow star, and blue circle corresponds to major, off, and minor axes pointings from GBT projects 20B-360,21B-324, and 15B-257. Yellow highlighted region correspond to region of expected emission.

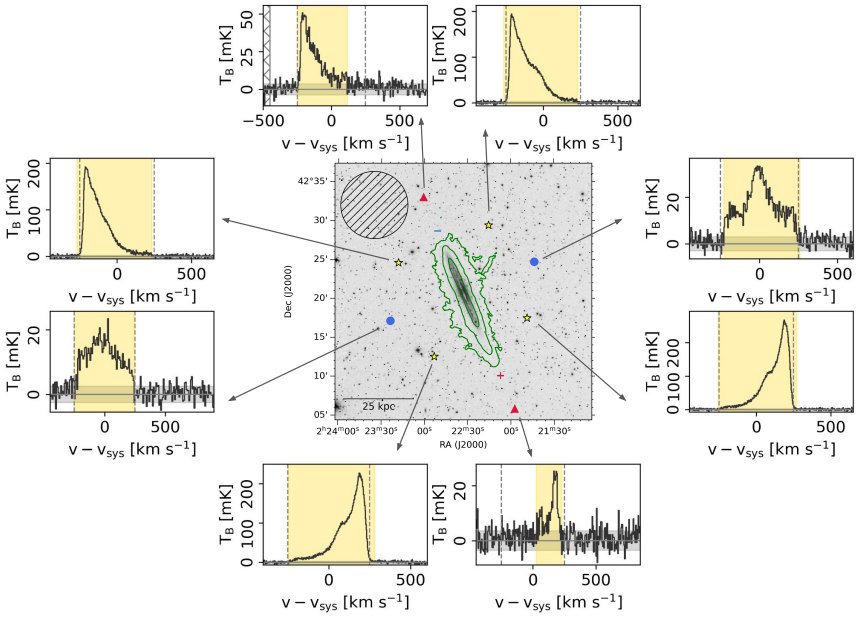

FIGURE 2: NGC 891 GBT spectra. Red triangle, yellow star, and blue circle corresponds to major, off, and minor axes pointings from GBT projects 20B-360,21B-324, and 15B-257. Yellow highlighted region correspond to region of expected emission.

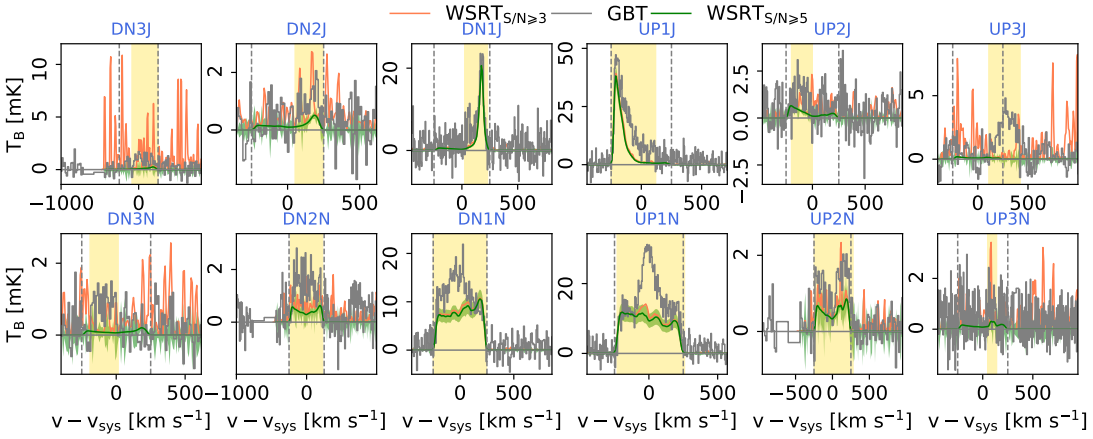

FIGURE 3: The GBT and WSRT spectra for our observed GBT pointings of NGC 891. The vertical yellow patch is the region where the H I emission is detected in the GBT data. The maximum rotational velocity of the H I disk is marked with vertical dashed gray lines. The green shaded regions around the green curves are the combined systematic uncertainty due to GBT beam circularization and masking the WSRT data cube at S/N> 4 or S/N> 6, and statistical uncertainty. The masking at S/N> 3 is discarded because it picks up a lot of spurious noise at UP/DN 2 and 3 pointings, and does not pick up any significant excess than the S/N> 4 masking at UP/DN 1 pointings ([2]).

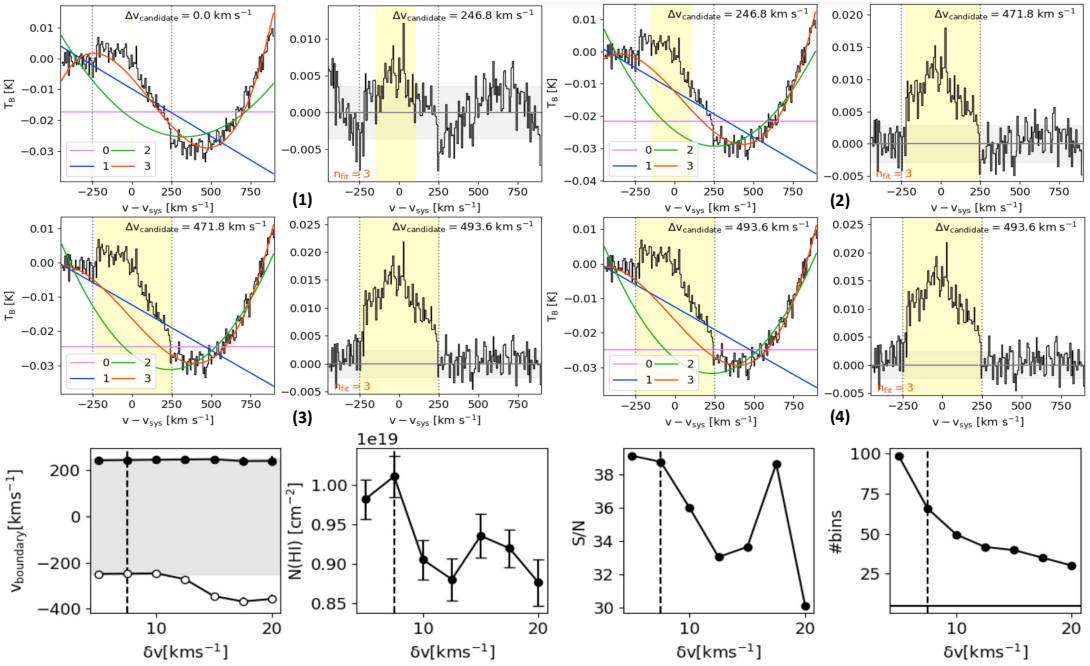

Illustration of the baseline fitting and subtraction routine for the 'DN1N' pointing of NGC 891 for $\delta v = 7.5$ km s^{-1} from D24.

FIGURE 4: **Top two rows:** Each iteration, noted in parentheses, consists of two panels. The left panels show the original spectrum with the candidate emission region indicated and the best-fit baselines of different polynomial orders plotted as colored lines. The right panels show the best-fit baseline-subtracted spectrum, with the best-fit polynomial order written in the bottom left corner. The vertical gray dotted lines denote the line width of the disk, $\Delta v_{\rm disk}$, for the target galaxy, NGC 891. The value of $\Delta v_{\rm candidate}$ (shown with vertical yellow bands) at the start and end of each iteration are noted as well. The fitting algorithm at this pointing converges in the fourth iteration. **Bottom row (from left to right):** $\Delta v_{\rm candidate}$, N(H I), S/N, and number of velocity channels ($=\Delta v_{\rm candidate}/\delta v$) of the candidate emission for different δv. In the leftmost panel, the gray horizontal band denotes $\Delta v_{\rm disk}$ of NGC 891. The filled and unfilled circles mark the upper and lower boundary of the candidate emission, respectively. In the rightmost panel, the horizontal line is drawn at 5, the threshold to identify a positive fluctuation as a candidate emission. The vertical dashed line in each panel corresponds to the optimum δv([2]).

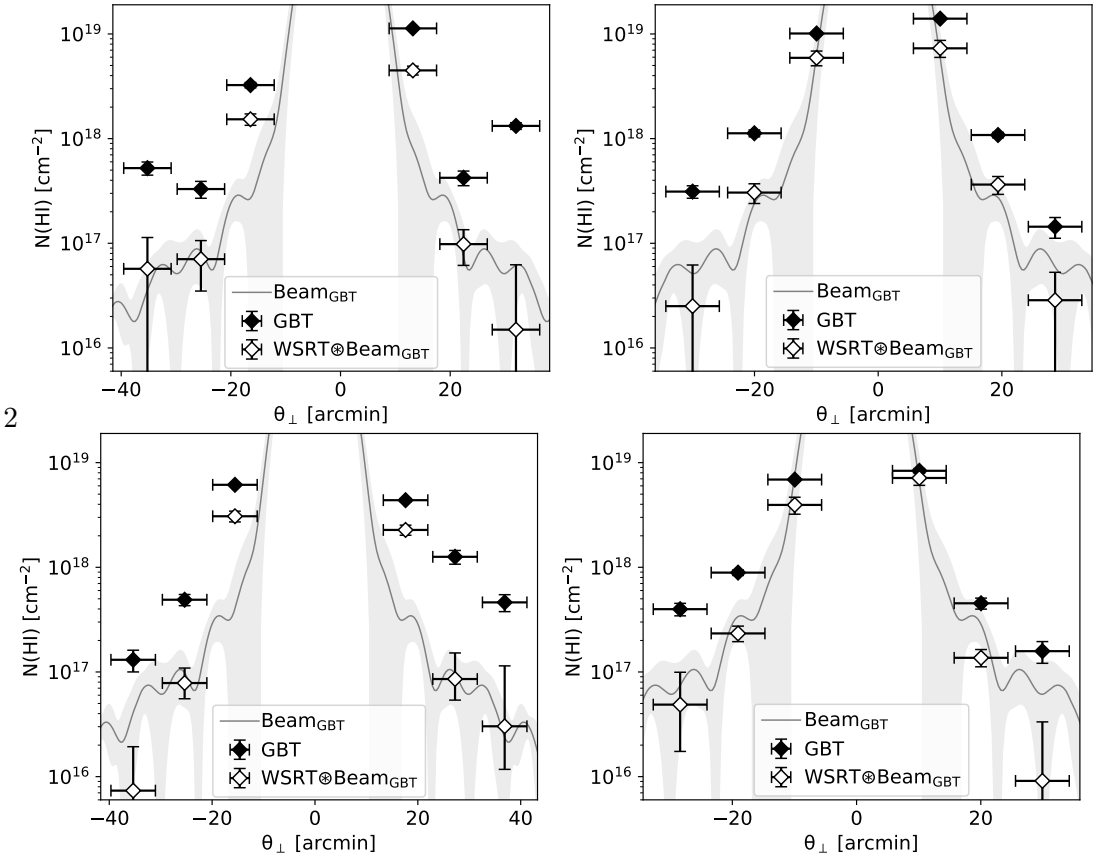

2

FIGURE 5: The radial N(H I) profile of NGC 891 (top) and NGC 4565 (bottom) along their major axes (left) and minor axes (right). The pointing at higher/lower declination than the galaxy disk are plotted at positive/negative angular separation from the galaxy center, respectively. The error bars along the y-axis include systematic uncertainties and statistical uncertainties. The error bars along the x-axis denote the GBT beam size. In our GBT data, systematic uncertainties come from the difference in T_{cal} across different sessions. In the WSRT data, systematic uncertainties come from the difference in masking threshold (S/N>4–5–6), and circularization of the GBT beam. The shaded region around the beam model is 1σ uncertainty in the beam response due to averaging the beam map to one dimension. The positive offset between our GBT data and the convolved WSRT data indicates the presence of diffuse circumgalactic H I([2]).

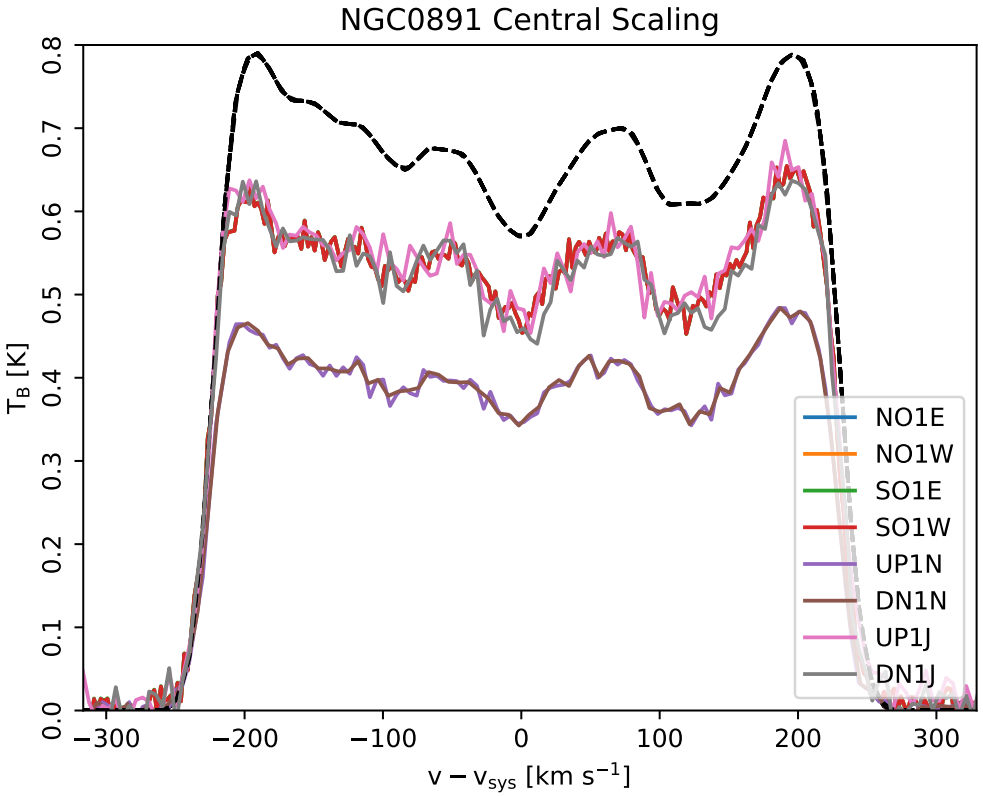

FIGURE 6: Velocity wise channel scaling using central pointing for each CGM pointing of NGC0891. Central pointings for respective CGM GBT pointings listed in legend. Black dashed line is WSRT 5σ convolved and masked central pointing.

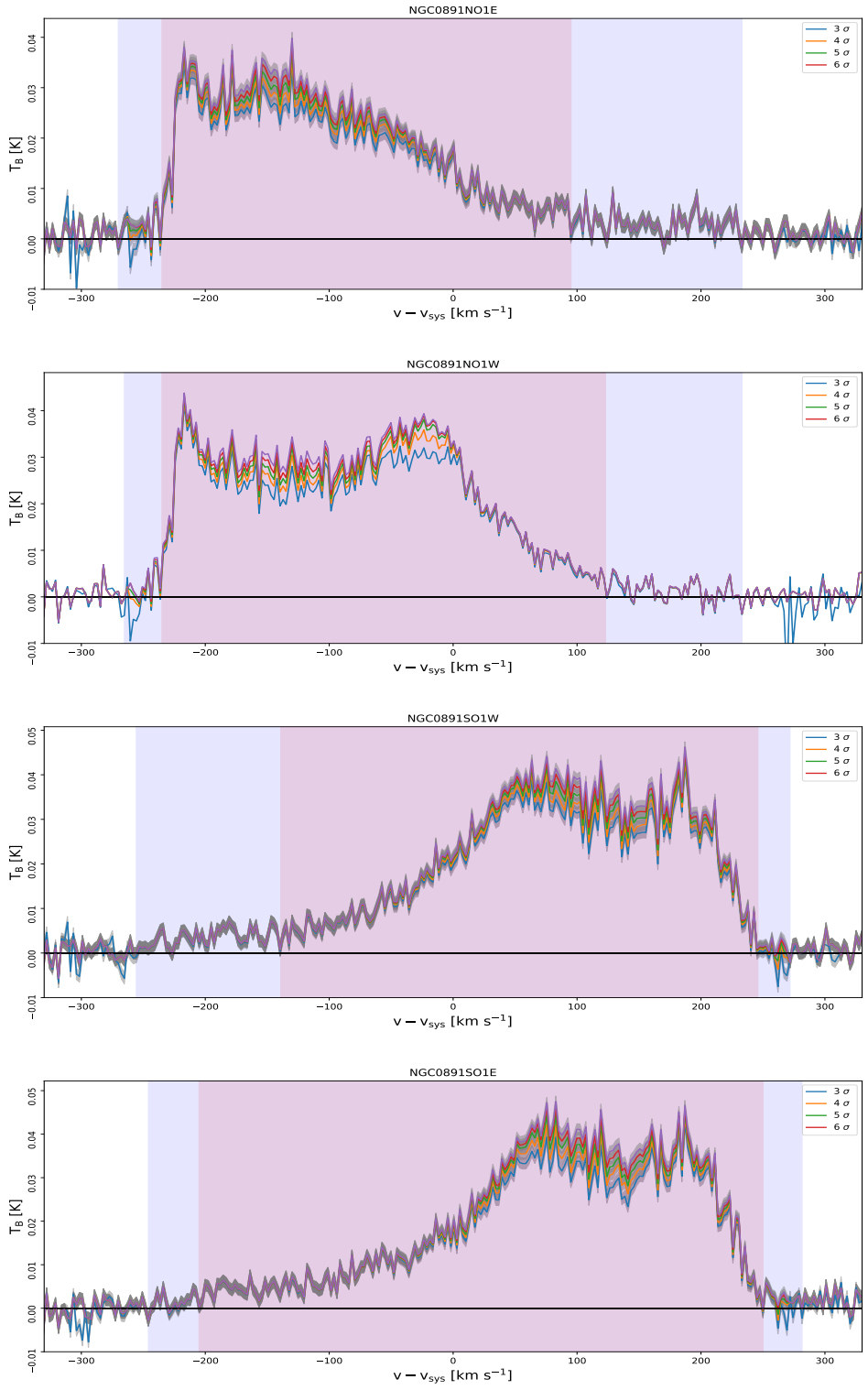

FIGURE 7: Diffuse spectra for NO1E (top), NO1W, SO1W, and SO1E(bottom) pointings brightness temperature against velocity for NGC 891. 3-6 σ statistical uncertainties plotted.

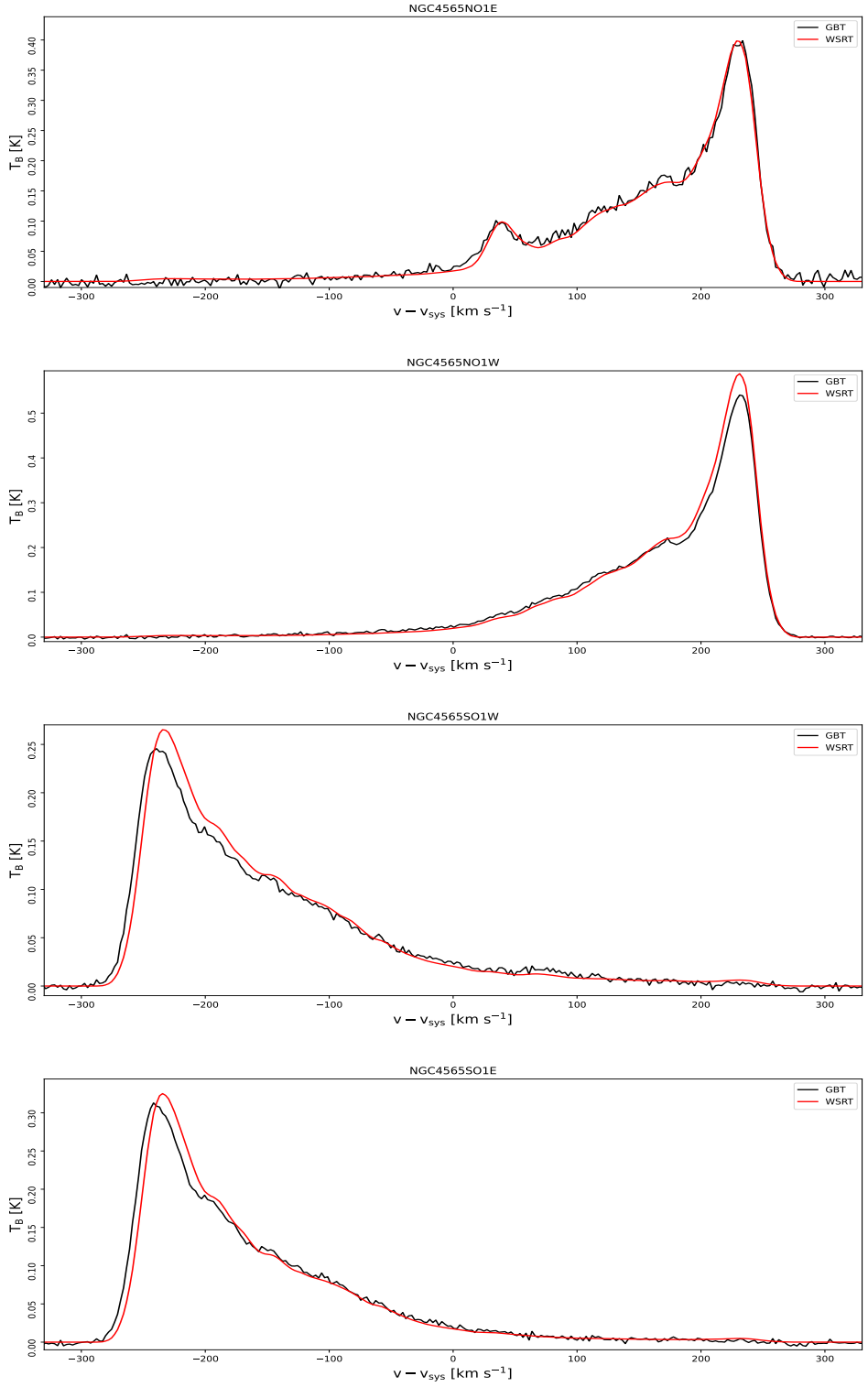

FIGURE 8: GBT (black) and WSRT (red) spectra for NO1E (top), NO1W, SO1W, and SO1E(bottom) pointings brightness temperature against velocity for NGC 4565.

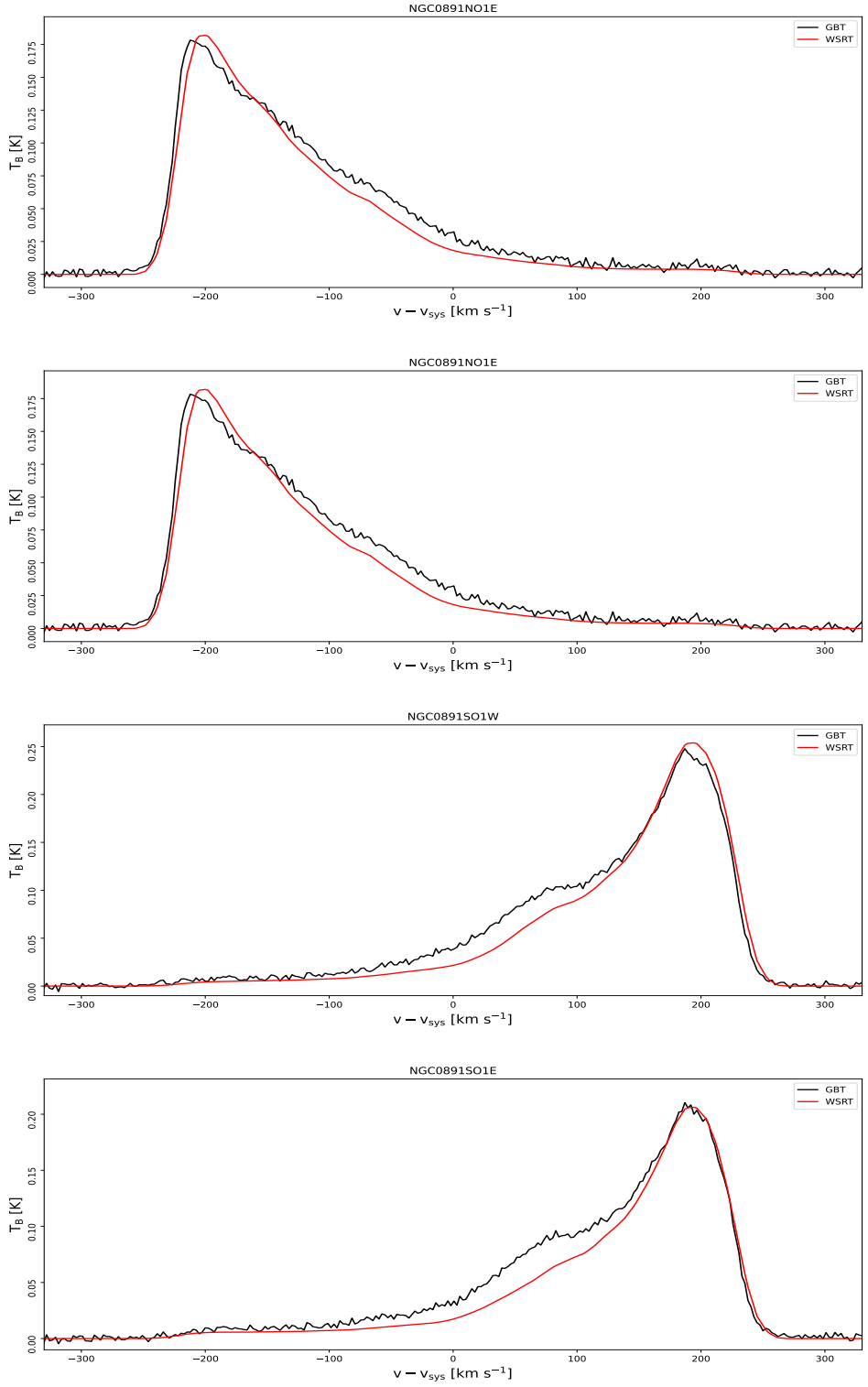

FIGURE 9: GBT (black) and WSRT (red) spectra for NO1E (top), NO1W, SO1W, and SO1E(bottom) pointings brightness temperature against velocity for NGC 891.

List of Tables

Pointing[(a)]	RA	DEC	$t_{\rm eff}$[(b)]	$T_{\rm sys}$	$\sigma_{T_{B,5}}$[(c)]	$d_\perp$	δv[(d)]	$\Delta v_{\rm emit}$[(e)]	$\Delta v_{\rm base}$[(f)]	$n_{\rm fit}$[(g)]
	(J2000)	(J2000)	(hrs)	(K)	(mK)	(kpc)	($\rm kms^{-1}$)	($\rm kms^{-1}$)	($\rm kms^{-1}$)	
NGC 891 ($2^h22^m33.6^s$, $42°20'58''$)										
NO1E	$2^h23^m18.06^s$	$+42°24'36''$	1.12	18.35	1.24	24.0	2.5	(-270, 233)	(-450, 650)	0
NO1W	$2^h22^m15.34^s$	$+42°29'25''$	1.12	18.36	1.25	24.3	2.5	(-265, 233)	(-450, 650)	0
SO1E	$2^h22^m53.18^s$	$+42°12'33''$	1.08	18.36	1.27	24.5	2.5	(-245, 281)	(-400, 600)	1
SO1W	$2^h21^m48.66^s$	$+42°17'29''$	1.08	18.35	1.27	24.1	2.5	(-255, 271)	(-450, 650)	1
NGC 4565 ($12^h36^m20.9^s$, $25°59'23''$)										
NO1E	$12^h36^m24.0^s$	$+26°\ 08'44''$	1.12	18.01	1.22	29.5	2.5	(-113, 282)	(-1000, 625)	3
NO1W	$12^h35^m39.4^s$	$+26°00'10''$	1.06	18.01	1.26	29.4	2.5	(-205, 280)	(-1000, 625)	3
SO1E	$12^h37^m02.6^s$	$+25°58'42''$	1.04	17.97	1.27	29.5	2.5	(-292, 139)	(-1000, 625)	3
SO1W	$12^h36^m18.3^s$	$+25°50'01''$	1.04	17.96	1.27	29.5	2.5	(-294, 209)	(-1000, 625)	3

TABLE 1: Data reduction

(*a*) "NO" and "SO" denote offset to higher and lower declination than the center of the target galaxy. Pointings along the off-axis at higher or lower right ascension offset of the target galaxy end with "E" and "W", respectively. Pointing "SO1E" is $1\times9.1'$ approximately 45° between principal H I disk axes as measured in interferometric surveys (see Figure 2), where $9.1'$ is the FWHM size of the GBT beam. The transverse distances of the pointings from the center of the target galaxy are provided in the 7th column, adopting a distance of 9.2 Mpc/10.8 Mpc for NGC 891/NGC 4565 from [3].

(*b*) Effective exposure time $t_{\rm eff} = t_{\rm on}\times t_{\rm off}/(t_{\rm on}+t_{\rm off})$. Where $t_{\rm on}$ and $t_{\rm off}$ are the integration times toward the on-source and the off-source pointings, respectively. To maximize $t_{\rm eff}$, we maintain $t_{\rm on}$ and $t_{\rm off}$ to be the same.

(*c*) The expected noise at $\delta {\rm v} = 5\,{\rm km\,s^{-1}}$ based on the radiometer equation.

(*d*) The velocity resolution at which the spectrum is smoothed.

(*e*) The velocity range over which the H I emission is detected.

(*f*) The velocity range that we use to estimate the baseline.

(*g*) The order of the best-fitted polynomial to describe the baseline.

Chapter 1

Introduction

1.1 Interstellar and Circumgalactic Medium

The majority of star formation in a spiral galaxy is constrained to the interstellar medium (ISM). Within the ISM, gas co-rotates and supernovae eject metals forging a nursery for future stars to be born. Using an ISM perspective alone, the amount of raw fuel needed to sustain star formation, H I , is insufficient on an orders of magnitude scale throughout cosmic time ([4],[5],[6]). This implies there must be an additional reservoir of H I gas contributing to the star formation in a galaxy. The region far outside a galaxies' disk, out to the virial radius, may play the key role in explaining this missing H I mass problem.

Around the disk of a spiral galaxy, there is a pervasive gas reservoir called the circumgalactic medium (CGM). The CGM is primarily hot and ionized but also hosts a small fraction of neutral hydrogen, HI. HI is the raw fuel for star formation and often traced using the spin flip transition at the 21 cm line. In the CGM, H I is tied up as clumpy high or intermediate velocity clouds and/or as diffuse low column density gas.

1.1.1 Existing CGM Observations

Work in the neutral phase CGM scene is often done through interferometery or single dish radio astronomy at the 21 cm line. Interferometric surveys such as the open source Hydrogen Accretion in LOcal GAlaxies Survey (HALOGAS; [7]), shallowly map the H I of nearby edge-on galaxies with a high angular resolution and point source sensitivity. The HALOGAS survey contributed a wealth of knowledge on the H I mass, morphology, kinematics, and extensions via filaments in extragalactic Milky Way analogs. Limited by the *uv* spacing problem, interferometers lack low surface brightness sensitivity needed to

detect low column density gas. Single dish telescopes, such as the Green Bank Telescope (GBT) probe all angular scales and achieve high surface brightness sensitivity. When compared at the same spatial and velocity resolution, single dish telescopes will detect all interferometers detect with the addition of low column density gas.

Observations of the CGM of local galaxies mapped using GBT obtained a 5 σ sensitivity of 10^{18} cm^{-2}over a 20 km^{-1} channel ([8],[9]) and variation amongst galaxies. The AMIGA project (Absorption Maps In the Gas of Andromeda) examined 48 quasar sightlines in the CGM of M31 using GBT and achieved a 5σ sensitivity of 10^{17} cm^{-2}. No HI emission was detected, omitting two sightlines passing over the Magellanic Stream, at an impact parameter of 23-340 kpc with the GBT beam corresponding to a physical length of 2 kpc ([10]). Implying, either M31 is an exception or successful H I detection requires a a greater covering fraction.

Observations of four local edge on galaxies using GBT were compared against HALOGAS, at the same veloicty and spatial resolution ([11]). No significant excess emission was detected in GBT at a 5σ GBT detection limit of 0.9–1.4 $\times$ 10^{18} cm^{-2}over a 20 km^{-1} channel. Implying, either these galaxies are also exceptions or the diffuse gas is at a sensitivity of $\leq 10^{18}$, meaning deeper observations are needed.

The predecessors of this work, Das et al. (2020) referred to as D20 [12] and Das et al. (2024) reffered to as D24 [2], observed two galaxies from Pingel et al. (2018) [11], NGC 891 and NGC 4565, using a deep stare with GBT. Observations in D20 and D24, stepped along the minor and major axes of each galaxy, integrated 3-4 hours each pointing, and achieved an unprecedented sensitivity of 5 σ sensitivity of 8.2 $\times$ 10^{16} cm^{-2}over a 20 km^{-1} line width. This thesis studies the major and off-axis of NGC 891 and NGC 4565 using GBT and HALOGAS data with the aim of detecting missing H I mass in the form of diffuse gas.

Examining 18 local MHONGOOSE galaxies with GBT, found 15 galaxy H I profiles do not truncate at large impact parameters ([13]). This work indirectly suggests the presence of diffuse H I beyond the disk in the CGM.

Existing work suggest physical mechanisms that govern the inflow of HI in the CGM may differ depending on the galactic disk properties such as morphology, mass, and star formation rate.

Chapter 2

Observations

2.1 GBT Projects

The Green Bank Telescope (GBT) is the most ideal candidate for exploring diffuse HI because of its unblocked aperture, high aperture efficiency, and high surface brightness sensitivity. We observe the CGM of galaxies NGC 891 and NGC 4565 in 21 cm using GBT projects 21B-324 (PI: Das), 20B-360 (PI: Das), and 15B-257 (PI: Leroy). These GBT projects target the off, major, and minor axes along of both galaxies. Previous studies by D20, and recently D24, examined the minor and major axes of both galaxies. The 21B-324 and 20B-360 projects contribute, in both galaxies, 4 new deep spectra along the off and major axes. Integrating spectra from D20 and D24 with the results from off axis observations, allows a 360 degree view of the H I CGM of each galaxy. In Figures 2 and 1, we add the first FWHM GBT beam sized step along each axis demonstrate this as blue circles from minor axis examination, red triangles from major axis examination, and yellow stars as off-axis examination.

2.1.1 Sample Selection

NGC 891 and NGC 4565 are prime targets for many reasons. In order to detect diffuse from "clumpy" emission, we require access to existing interferometric surveys. Motivated by Pingel et al. 2018, D20, and Sardone et al 2021, interferometric maps can be convolved with the GBT beam and comapred to GBT spectra. NGC 891 and NGC 4565 are both open source in the HALOGAS survey; which is a deep (10^{19} cm^{-2}) map of each target galaxy. To study the azimuthal distribution of H I in the CGM, we need to observe principal and off axes, limiting us to highly inclined edge-on galaxies. Additionally, we require the galaxies to be nearby but not so close as to have a shallow covering fraction

of CGM emission. We also require the systemic velocities to be sufficiently different from the Milky Way's emission to allow for clear signal detection and baseline subtraction. Lastly, we require a clear spiral disk vs CGM delineation.

We determined the pointings along each galaxy's axes based on previous examinations of their disks. Along the major and minor axes, we step out 3 GBT FWHM beam sizes from the center, referred to as UP1J-DN3J and UP1N-DN3N, respectfully. The minor axis is closer to center due to disk and CGM truncation, while major axis is farther because of larger impact parameter disk truncation. The off-axis pointings are defined to be about 45 degrees between the minor (referred to as N) and major axis (referred to as J), ensuring they never intersect the disk. Along the off-axes, we step one GBT FWHM beam size, labeling high declination pointings as north (NO) and high right ascension as east (E), yielding pointings such as NO1E, SO1E, SO1W, and NO1W relative to each galaxy's orientation.

We ensure pointings are not in the line of sight of particularly bright sources (OR known HI emitters). Unfortunately, some are inevitable such as the filament in NGC 891 NO1W, and the companion/satellite galaxy in the SO1W of NGC 4565. We select the flux calibration sources to be 3C123 and 3C286 for NGC891 and NGC 4565, respectively. It is from these flux calibration sources that we determine systematic uncertainties.

Chapter 3

GBT Data Reduction

Data is obtained from 20 sessions in both 21B-324 and 20B-360 GBT projects at the 21 cm (1.42 GHz). In both projects, we leverage two polarization position switching techniques using the L-band receiver and Versatile GBT Astronomical Spectrometer (VEGAS; bandwidth = 23.5 MHz) as the backend. We select the flux calibration sources to be 3C123 and 3C286 for NGC891 and NGC 4565, respectively. Off-sources are 1.5° off from the disk at varying RA but fixed declination due to additional error arising from overhead time in changing the declination.

We use a manual GBTIDL reduction pipeline[1] to reduce the position switched spectra. From GBTIDL, we extract the spectral weight, effective integration time (t_{eff}), and average system temperature (T_{sys}), for both polarizations in each session. We visually remove radio frequency interference (RFI) channels, then linearly interpolate these channels using the adjacent channels.

A noise tube calibrator sets the gain factor which is used to convert from photon count and brightness temperature in kelvin. This calibration temperature, T_{cal} , comes from using specific calibration sources and is averaged over the entire bandpass. T_{cal} varies across polarization and across receiver and is calculated using the aperture efficiency and atmospheric opacity at zenith using GBTIDL. We report an average T_{cal} across both polarizations and each pointing in Table 1, and use T_{cal} later as the multiplicative systematic uncertainty in the GBT observations.

We stack all sessions for one pointing in each polarization. After stacking, we weight by t_{eff}/T_{sys}^2 to obtain a mean spectra for both polarizations and each pointing. We average across the polarizations into one spectra. We subtract the systemic velocity

[1]Developed by Sanskriti Das

of the galaxy, so all spectrum are in the reference frame of the respective galaxy. The velocity axis is centered on the galaxy's systemic velocity.

Once the GBT data is reduced and stacked, we fit a baseline to the spectra using the method outlined in D24, see Figure 4. For off-axis data, we allow the polynomial to range from 0-3 [2]. In D24, we allowed our velocity resolution to be 5-20 kms^{-1}, smoothing out for farther away pointings. In the off-axis sample, we find strong signals, high SNR, and relatively simple baselines (especially compared to the signal). We restrict our velocity resolution to 2.5 kms^{-1}. Before, we had sacrificed kinematic information in order to preserve the shape of the signal. With significant strong signals, we were able to preserve kinematic information while still having a high SNR from our velocity resolution. When comparing 2.5 and 5 kms^{-1}, we found no significant improvement. Our SNR in most cases ranges from 280-380, implying the detection of strong signals. As a result, we decided to go with the smallest velocity width reasonable, 2.5kms^{-1}. In terms of actually fitting the baseline, we input a prior choice of velocity baseline range and range of emission. We use an iterative polynomial fitting baseline method using our priors and as described in D24 and in Figure 4. The baseline subtracted spectra is used for further HALOGAS comparison.

GBT project 21A-377[3] observed the CGM along the minor axes of four nearby edge-on galaxies, UGC 2082, UGC 4278, NGC 5023, and NGC 5229. This project is the next step in improving the sample size of the D20 and D24 series. Successful reductions of these galaxies are complete and will be featured in an upcoming publication.

[2] Order 3 used only in NGC 4565, which is well characterized with a wavy baseline
[3] Not included in this work though within the scope of the project

Chapter 4

WSRT Data Reduction

It is well known that interferometers cannot probe larger angular scales due to the *uv* spacing problem. The angular scale is inversely proportional to the configuration size, meaning a tighter configuration allows us to probe larger angular scales. The tightest configuration in Westerbork Synthesis Radio Telescope (WSRT) has a baseline length of 36 m, which directly translates to a maximum of 20 arcmin angular scale.

Single-dish telescopes have full *uv* coverage meaning they can probe all angular scales. To only examine diffuse H I , we must compare our GBT single dish observations with existing interferometric data. To do this, we leverage accessible data from the WSRT from the HALOGAS survey. To convert WSRT to within the same resolution and velocity space as GBT, we estimate mask and convolve WSRT as done similarly in D20 and D24, described in further detail in the Appendix. We add a more rigorous method of scaling the brightness temperatures, which is discussed in the below.

After converting WSRT to be within the same velocity space as GBT, we mask the data cubes of thresholds from 1-7 using methods described in D24. In D24, we scaled based on the one central pointing, from all sessions, to determine the discrepancy between HALOGAS and GBT. In this work we scale each pointing with its central pointing, i.e. the central pointing from the sessions the respective pointing, and scale across all channels.

4.0.1 WSRT Cubes

In order to compare GBT and WSRT results, we need to make adjustments to WSRT cubes in order to make sure the angular resolution, velocity, and brightness temperatures are scaled properly to be comparable to GBT. Using the following procedures, we adjust the cubes:

Noise Estimation: Similar to D20 and D24, we determine a global noise for each low-resolution WSRT cube (which are open source and available on the WSRT HALOGAS website). To do this, we set two regions of exclusion (r=20 arcmin and 30 arcmin). We fit a Gaussian to the negative histogram values outside of the regions of exclusion and determine the fit's standard deviation. Since diffuse CGM emission in the HALOGAS cubes is likely to be faint, we avoid fitting the positive values because we may mistake a faint signal to be noise. Fitting the non-physical negative flux values allows us to accurately extract a global noise and preserve possible faint signals. The minimum standard deviation of the two regions is set to be the global noise for the cube.

Primary Beam Correction: We apply a primary beam correction factor to account for the spatially varying noise present in the data cubes. This procedure is the same as D20 and D24.

Masking: Especially near the disk, unmasked HALOGAS spectra are contaminated with noise that may over estimate the column density of HI observed by WSRT. Using the same procedure as D24, we mask the primary beam corrected cubes using signal to noise thresholds (S/N) ranging from 1 to 7 sigma, plotted in Figure 7. Functionally, we examine the pixel in each velocity channel and retain the pixel value if it, and at least one adjacent channel, is greater than our S/N. Any channel and an adjacent channel failing the S/N threshold test, we nullify.

GBT Beam: We circularize the GBT beam by azimuthally average the GBT beam response in 1D. The GBT beam varies in antenna position angle throughout observations which introduces additional systematic uncertainty. We report the multiplicative systematic uncertainties due to beam asymmetry in Table 1.

Convolution: We convolve the masked HALOGAS cubes with the circularized GBT beam and extract spectra at each S/N threshold.

From the above procedures, we take the main result to be the 5σ masked spectra and obtain the statistical uncertainty lower bound to be 4σ and upper bound to be 6σ . In the Figure 7, we plot the diffuse spectra including all σ levels.

We improve our analysis from D20 and D24 to include additional steps to compare HALOGAS and GBT.

Velocity Wise Scaling: As mentioned previously, we subtract the systemic velocity of each galaxy in HALOGAS to obtain the spectra within the rest frame of the galaxy–especially good for demonstrating co-rotation. After subtracting the systemic velocities, we notice the width of HALOGAS emission is narrower than GBT. To remedy this, we

align the rising (left) edge of HALOGAS with GBT by subtracting an additional "edge correct factor".

1. **NGC 891:** We notice the "edge correct factor" is approximately the width of two velocity bins, specifically 5.0 kms^{-1}. By subtracting the edge correcting factor, the edges of HALOGAS and GBT line up and the width aligns. **ref image**
2. **NGC 4565:** We notice the "edge correct factor" is approximately the width of two velocity bins, specifically -5.0 kms^{-1}. However, this was insufficient for NGC 4565. We find subtracting the single edge correction factor does not adequately line up the falling (right) edge of the emission, meaning the width of the emission in each pointing of WSRT is narrower than GBT but is not consistent across each pointing.

Brightness Temperature Scaling: To equally compare between HALOGAS and GBT, we apply a scaling factor in brightness temperature. As shown in Figure BLAH, HALOGAS observations of the central pointing differs from GBT by a multiplicative factor greater than one. In D20 and D24 we obtained this brightness temperature scaling factor from the average difference in integrated intensity from HALOGAS and GBT. By averaging the difference, we assume the scaling is uniform across all velocity channels– resulting in an overall loss of information about channel wise difference. In this work, we determine the scaling factor between HALOGAS and GBT in each channel plotted in Figure 6.

Chapter 5

Results

The work of this thesis is deeply interwined with the results from D24 and upcoming, Rickel et al. (2024) in preparation. Below, we discuss the findings from D24.

In Figure 5, we examine the calculated column density as a function of galactocentric radius, and find successful detections in nearly all pointings. Observations along the major axis resulting in H I detections out to 90-120 kpc from the centers of NGC 891 and NGC 4565 at a 5 σ sensitivity of 4 x 10^{17} cm^{-2}. Directly comparing GBT observations with HALOGAS, we find a measurable excess in GBT at a factor of 2 greater than WSRT. Reinforcing that interferometers are not sensitive to low column density gas. Considering the mass of H I from D20, the extended H I phase along the minor and major axes accounts for 5.2 $\pm$ 0.9% and 2.0 $\pm$ 0.8% of the total galaxy H I mass, for NGC 891 and NGC 4565 respectively.

In the off axis, we successfully reduce the data and obtain spectra of the respective pointings. We plot the GBT, convovled masked and reduced 5 σ WSRT in Figure 9 and Figure 8. Analysis, in the form of calculating column density, mass of H I , and velocity dispersion will occur in the related publication of this thesis work.

Bibliography

[1] Sanskriti Das, Amy Sardone, Adam K. Leroy, Smita Mathur, Molly Gallagher, Nickolas M. Pingel, D. J. Pisano, and George Heald. Detection of the Diffuse H I Emission in the Circumgalactic Medium of NGC 891 and NGC 4565. , 898(1):15, July 2020. doi: 10.3847/1538-4357/ab97b9.

[2] Sanskriti Das, Mary Rickel, Adam Leroy, Nickolas M. Pingel, D. J. Pisano, George Heald, Smita Mathur, Joshua Kingsbury, and Amy Sardone. Detection of diffuse H I emission in the circumgalactic medium of NGC 891 and NGC 4565 - II. , 527 (4):10358–10375, February 2024. doi: 10.1093/mnras/stad3892.

[3] G. Heald, G. Józsa, P. Serra, L. Zschaechner, R. Rand, F. Fraternali, T. Oosterloo, R. Walterbos, E. Jütte, and G. Gentile. The Westerbork Hydrogen Accretion in LOcal GAlaxieS (HALOGAS) survey (Corrigendum). I. Survey description and pilot observations. , 544:C1, August 2012. doi: 10.1051/0004-6361/201015938e.

[4] Renzo Sancisi, Filippo Fraternali, Tom Oosterloo, and Thijs van der Hulst. Cold gas accretion in galaxies. , 15(3):189–223, Jun 2008. doi: 10.1007/s00159-008-0010-0.

[5] Fabian Walter, Chris Carilli, Marcel Neeleman, Roberto Decarli, Gergö Popping, Rachel S. Somerville, Manuel Aravena, Frank Bertoldi, Leindert Boogaard, Pierre Cox, Elisabete da Cunha, Benjamin Magnelli, Danail Obreschkow, Dominik Riechers, Hans-Walter Rix, Ian Smail, Axel Weiss, Roberto J. Assef, Franz Bauer, Rychard Bouwens, Thierry Contini, Paulo C. Cortes, Emanuele Daddi, Tanio Diaz-Santos, Jorge González-López, Joseph Hennawi, Jacqueline A. Hodge, Hanae Inami, Rob Ivison, Pascal Oesch, Mark Sargent, Paul van der Werf, Jeff Wagg, and L. Y. Aaron Yung. The Evolution of the Baryons Associated with Galaxies Averaged over Cosmic Time and Space. , 902(2):111, October 2020. doi: 10.3847/1538-4357/abb82e.

[6] P. Kamphuis, E. Jütte, G. H. Heald, N. Herrera Ruiz, G. I. G. Józsa, W. J. G. de Blok, P. Serra, A. Marasco, R. J. Dettmar, N. M. Pingel, T. Oosterloo, R. J. Rand, R. A. M. Walterbos, and J. M. van der Hulst. HALOGAS: Strong constraints on

the neutral gas reservoir and accretion rate in nearby spiral galaxies. , 668:A182, December 2022. doi: 10.1051/0004-6361/202140704.

[7] G. Heald, G. Józsa, P. Serra, L. Zschaechner, R. Rand, F. Fraternali, T. Oosterloo, R. Walterbos, E. Jütte, and G. Gentile. The Westerbork Hydrogen Accretion in LOcal GAlaxieS (HALOGAS) survey. I. Survey description and pilot observations. , 526:A118, Feb 2011. doi: 10.1051/0004-6361/201015938.

[8] D. J. Pisano. Green Bank Telescope Observations of Low Column Density H I around NGC 2997 and NGC 6946. , 147(3):48, Mar 2014. doi: 10.1088/0004-6256/147/3/48.

[9] W. J. G. de Blok, K. M. Keating, D. J. Pisano, F. Fraternali, F. Walter, T. Oosterloo, E. Brinks, F. Bigiel, and A. Leroy. A low H I column density filament in NGC 2403: signature of interaction or accretion. , 569:A68, Sep 2014. doi: 10.1051/0004-6361/201423880.

[10] J. Christopher Howk, Christopher B. Wotta, Michelle A. Berg, Nicolas Lehner, Felix J. Lockman, Zachary Hafen, D. J. Pisano, Claude-André Faucher-Giguère, Bart P. Wakker, J. Xavier Prochaska, Spencer A. Wolfe, Joseph Ribaudo, Kathleen A. Barger, Lauren Corlies, Andrew J. Fox, Puragra Guhathakurta, Edward B. Jenkins, Jason Kalirai, John M. O'Meara, Molly S. Peeples, Kyle R. Stewart, and Jay Strader. Project AMIGA: A Minimal Covering Factor for Optically Thick Circumgalactic Gas around the Andromeda Galaxy. , 846(2):141, September 2017. doi: 10.3847/1538-4357/aa87b4.

[11] N. M. Pingel, D. J. Pisano, G. Heald, T. H. Jarrett, W. J. G. de Blok, G. I. G. Józsa, E. Jütte, R. J. Rand, T. Oosterloo, and B. Winkel. A GBT Survey of the HALOGAS Galaxies and Their Environments. I. Revealing the Full Extent of H I around NGC 891, NGC 925, NGC 4414, and NGC 4565. , 865(1):36, Sep 2018. doi: 10.3847/1538-4357/aad816.

[12] Sanskriti Das, Smita Mathur, and Anjali Gupta. The Warm-Hot, Extended, Massive Circumgalactic Medium of NGC 3221: An XMM-Newton Discovery. , 897(1):63, July 2020. doi: 10.3847/1538-4357/ab93d2.

[13] Amy Sardone, D. J. Pisano, N. M. Pingel, A. Sorgho, Claude Carignan, and W. J. G. de Blok. A Census of the Extended Neutral Hydrogen around 18 MHONGOOSE Galaxies. , 910(1):69, March 2021. doi: 10.3847/1538-4357/abde45.